CHINESE OPTICS LETTERS

Vol. 21, No. 11 | November 2023

Femtosecond laser filamentation in simulated atmospheric turbulence [Invited]

Jiewei Guo (郭杰伟)[1,2,†], Lu Sun (孙 陆)[1,2,†], Yuezheng Wang (王悦政)[1,2], Jiayun Xue (薛嘉云)[1,2], Zhi Zhang (张 智)[1,3*], Haiyi Liu (刘海毅)[1,2], Shishi Tao (陶诗诗)[1,2], Wenqi Qian (钱文启)[1,2], Pengfei Qi (齐鹏飞)[1,2], Lie Lin (林 列)[1,3], and Weiwei Liu (刘伟伟)[1,2]

[1] Institute of Modern Optics, Eye Institute, Nankai University, Tianjin 300350, China

[2] Tianjin Key Laboratory of Micro-scale Optical Information Science and Technology, Tianjin 300350, China

[3] Tianjin Key Laboratory of Optoelectronic Sensor and Sensing Network Technology, Tianjin 300350, China

*Corresponding author: zhangzhi@nankai.edu.cn

Received September 7, 2023 | Accepted October 4, 2023 | Posted Online November 9, 2023

The effects of turbulence intensity and turbulence region on the distribution of femtosecond laser filaments are experimentally elaborated. Through the ultrasonic signals emitted by the filaments, it is observed that increasing turbulence intensity and an expanding turbulence active region cause an increase in the start position of the filament and a decrease in filament length, which can be well explained by theoretical calculation. It is also observed that the random perturbation of the air refractive index caused by atmospheric turbulence expands the spot size of the filament. Additionally, when the turbulence refractive index structure constant reaches $8.37 \times 10^{-12}\ \mathrm{m}^{-2/3}$, multiple filaments are formed. Furthermore, the standard deviation of the transverse displacement of filament is found to be proportional to the square root of the turbulent structure constant under the experimental turbulence parameters in this paper. These results contribute to the study of femtosecond laser propagation mechanisms in complex atmospheric turbulence conditions.

Keywords: femtosecond laser filamentation; turbulence.

DOI: 10.3788/COL202321.110004

1. Introduction

When femtosecond laser pulses propagate in transparent media, including gases, liquids, and solids, the beam can propagate over a long distance without diffraction along with a self-generated plasma channel, named filament[1–3]. The formation of the optical filaments is the balancing result of the dynamic counteraction between the optical Kerr effect-induced self-focusing and the defocusing[2–4]. The femtosecond laser filamentation can give rise to a nearly constant laser intensity as high as $10^{14}\ \mathrm{W/cm^2}$ over a long distance ranging from meters to kilometers in the atmosphere[5,6]. The ultrastrong laser intensity is high enough to induce remote ionization and fragmentation of molecules, giving rise to characteristic fingerprint fluorescence emissions and providing an opportunity for investigating strong-field molecule interaction in complicated environments, especially with remote sensing[7–9]. The length, position, and intensity of the femtosecond laser filament can be effectively controlled by initial laser parameters and the spatiotemporal shaping of the pulses[10–12]. Therefore, the versatile femtosecond laser filament technology demonstrates a great potential for the remote sensing of air pollutants and hazardous substances such as explosives and chemical weapons. However, the remote sensing of multicomponent pollutants and targets remains challenging, owing to the inevitable turbulence and ultralow concentration.

Femtosecond laser filaments are inevitably affected by atmospheric turbulence in air, which poses an unavoidable problem for the practical application of femtosecond laser filaments. Recently, some studies have been reported on the effect of atmospheric turbulence on femtosecond laser filament formation[13,14]. Turbulence induces the fluctuation of the surrounding air density, consequently causing refractive index variations and distorting optical waves, which leads to a transverse stochastic distribution, increased filament counts, and expanded spot size[15–17]. Moreover, the onset of filamentation has been observed to be contingent upon different conditions[18–21]. These trivial changes in filamentation have a great impact on sensitivity during remote sensing due to the ultrastrong nonlinear effect. Hence, the spatial distribution of filament during their propagation in a turbulent atmosphere plays a critical role in remote sensing. The dynamics of long-range femtosecond laser filamentation in atmospheric turbulence is not clear yet. The empirical formulas describing turbulence effects on the pointing

stability of optical filaments are yet to be reported, which will be also a crucial issue for achieving a high-performance remote air laser.

Here, we focus on the femtosecond laser filamentation in turbulence with a distance of 30 m. We carefully examined the impact of turbulence intensity and interacted region on the onset distance, length, intensity, and diameter of the filaments. The increased turbulent intensity and interacted region increased the onset distance and decreased the length of the filament, which can be explained well by theory. Furthermore, the empirical formulas describing the relationship between the standard deviation of transverse displacement of filament and turbulence intensity in different regions are proposed.

2. Experimental Setup

The experimental remote sensing setup using filaments is illustrated in Fig. 1. A commercial femtosecond laser system (Legend Elite, Coherent Inc.) delivers 60 fs pulses at the central wavelength of 800 nm, with the maximum pulse energy of 4 mJ at a repetition rate of 500 Hz. The laser pulse output from the laser system was focused by a lens group comprising a concave lens (L1) with a focal length of −150 mm and a convex lens (L2) with a focal length of 203 cm. The geometrical focus of the lens group is located 30 m away from the convex lens. The position of L2 is defined as the original point of the propagation distance, $z = 0$ m. Along the propagation of the femtosecond laser pulses, air turbulence is introduced by the turbulent blower, which consists of a 30 m-long air duct with two high-speed centrifugal turbo blowers (1.2 kW) placed above the laser propagation. The size 20 cm × 40 cm refers to each outlet of the duct, which is shown in Fig. 1(a). By manipulating the airflow outlet below the duct, we have the capability to modify the turbulence region. The location of L2 is specified as the zero point of the region of turbulent action; the turbulence position with respect to the laser region is shown in Fig. 2(e).

During photo-ionization, free electrons were ejected with high kinetic energy at the order of eV, which corresponded to an initial electron temperature of the order of 10^4–10^5 K[22]. The energy transfer between the hot free-electron gas and the heavy species in the ambient gas occurred by collisions resulting in a hot gas column after the recombination of the plasma. The expansion of such a hot gas column led to an acoustic wave (AW) emission that could be detected by a microphone. To clarify the onset and length of the filament, as shown in Fig. 1(b), an ultrasonic probe (V306, Olympus. Ltd.) combined with an amplifier (5072PR, Olympus. Ltd.) and an oscilloscope (DPO3034, Tektronix Inc.) is placed at a distance of 1 cm perpendicular to the propagation axis to collect the ultrasonic wave emitted from the optical filament. The typical time-domain ultrasonic signal is shown in Fig. 1(d). Because the length of the optical filament (~28 cm) is much longer than the spatial resolution (~0.87 cm) of the ultrasonic microphone, the microphone is mounted on an electrically driven sliding rail and moved parallel to the laser propagation direction to measure

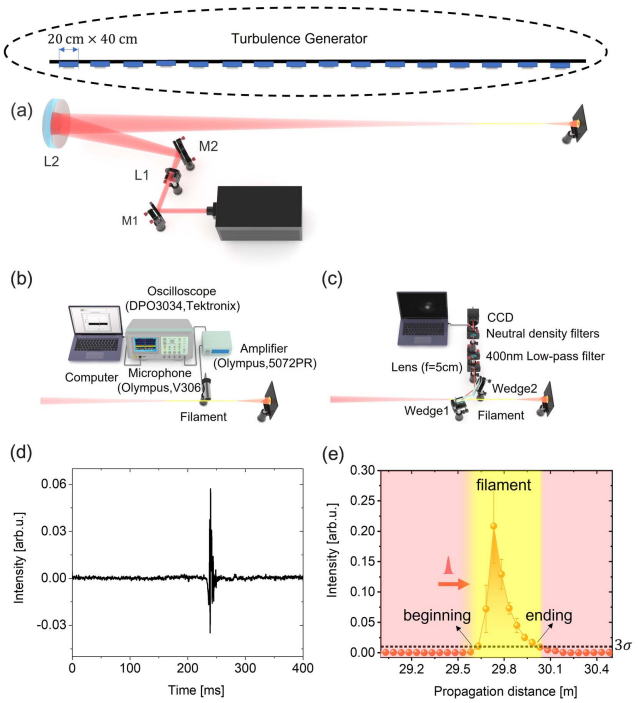

Fig. 1. Schematic diagram. (a) Schematic diagram of the experimental setup; (b) experimental setup for recording ultrasonic signal induced by filament; (c) experimental setup for recording the cross section of filaments; (d) time-domain diagram of the filament-excited ultrasonic signal; (e) longitudinal acoustic intensity along the filament without turbulence (dashed line is 3σ).

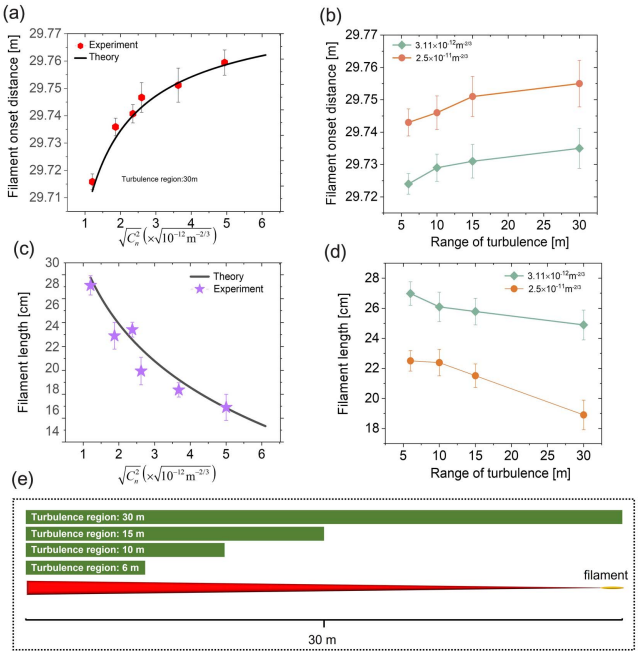

Fig. 2. (a) Onset position and (c) length of filaments as a function of turbulence refractive index structure constant within the 30 m region; (b) onset position and (d) length of filaments as a function of turbulence region; (e) schematic of turbulent regions and femtosecond lasers.

the length and distribution of the filament point by point. The spatial step of the microphone is 2.5 cm.

To analyze the distribution of the filament cross section, as indicated in Fig. 1(c), two fused silica wedges are inserted into the laser beam path, both at grazing angles, yielding a reflectivity of about 10% at each front surface. Therefore, after two surface reflections, the laser intensity is reduced to approximately 1%. The cross sections of the laser beam are then detected by a CCD camera through a calibrated 1:4 imaging setup. The exposure time of the CCD is set at 1 ms to capture a single pulse for each picture. The neutral density filters are placed in front of the CCD camera to further attenuate the laser intensity.

By adjusting the frequency of the blower and the location of the outlets, we can control the intensity and position of turbulence, respectively. The turbulence intensity is expressed by the refractive index structure constant[23]: $C_n^2 = \sigma^2 \phi^{1/3}/2.91L$, where σ is the standard deviation of the angle of arrival. The beam diameter and the length of the turbulence region are denoted by ϕ and L, respectively. To calculate the refractive index structure constant, a low-power continuous-wave He–Ne laser was used, which propagates along the same path as the femtosecond laser pulses. We quantified the refractive index structure constant of the artificial turbulence, and the turbulence refractive index structure constants are $1.68 \times 10^{-12}\ \mathrm{m}^{-2/3}$, $3.11 \times 10^{-12}\ \mathrm{m}^{-2/3}$, $3.83 \times 10^{-12}\ \mathrm{m}^{-2/3}$, $8.37 \times 10^{-12}\ \mathrm{m}^{-2/3}$, $1.61 \times 10^{-11}\ \mathrm{m}^{-2/3}$, and $2.5 \times 10^{-11}\ \mathrm{m}^{-2/3}$, which relatively correspond to atmospheric turbulence[15,21].

The distribution of ultrasonic signal along the filament without turbulence as a function of the propagation distance z is shown in Fig. 1(e), where the start and end positions of the filament are defined at the positions where the ultrasonic signal value is just over the dashed line according to the 3σ rule (σ, the standard deviation of the background noise intensity). To reduce the error of experimental measurements, the measurement in Fig. 1(e) is the average result of 10 measurements. The start position of the filament is about 29.71 m.

3. Results and Discussion

First, the longitudinal distribution of the filament under different turbulent conditions is investigated. Figure 2(a) depicts the recorded onset distance of filaments with different turbulent intensities within a turbulent region of 30 m, which can significantly modulate the filamentation dynamics and the acoustic emission. It can be clearly observed that the increased turbulent refractive index structure constant increases the onset distance of the filament. It is worth noting that the minimum turbulence refractive index structure constant depicted in Fig. 2(a) reflects the air disturbance within the experimental environment. Furthermore, it is observed that altering the region of turbulent activity does not modify the correlation between the location of filament initiation and the intensity of turbulence (Fig. S1 in Supplementary Material).

Nevertheless, we can see that the relationship between the onset position of the filament and the square root of the turbulent structure constant is not linear, which may be due to the fact that the formation of the filament is a nonlinear process and the onset position of the filament is related to the self-focusing threshold power of the beam collapse. Turbulence has the potential to influence the self-focusing threshold power of femtosecond laser filamentation. The relationship between the turbulent refractive index structure constant and the self-focusing threshold power has been studied theoretically, and air turbulence is predicted to increase the power threshold (P_c) for beam collapse[21], which can be described as $\frac{P_c}{P_{cr}} = 1 + \frac{3}{4}k_0^2 a^2 (\frac{aC}{2})^{\frac{2}{3}}$, where $P_{cr} = \frac{3.77\lambda^2}{8\pi n_2 n_0}$ is the critical power threshold and $C = 4.38 l_0^{-1/3} C_n^2 (1 - (1 + 17.5\frac{a^2}{l_0^2})^{-1/6})$. Therefore, we can obtain the relationship between the self-focusing threshold power under the turbulent and the filament starting position. Consequently, the air turbulence impacts the self-focusing distance of the filament, i.e., $Z_f = \frac{0.367 k_0 a^2}{\sqrt{(\sqrt{\frac{P}{P_c}} - 0.852)^2 - 0.0219}}$. Additionally, the self-focal distance (Z_f) will be modified under different external focusing conditions, i.e., $Z_f' = \frac{Z_f f}{Z_f + f}$[24]. Figure 2(a) indicates that the experimental and theoretical results are in good agreement.

Then we explore the impact of the turbulent action region on the filament start position under two experimental conditions: a maximum of $2.5 \times 10^{-11}\ \mathrm{m}^{-2/3}$ and a minimum of $3.11 \times 10^{-12}\ \mathrm{m}^{-2/3}$ for the turbulence refractive index structure constant. As depicted in Fig. 2(b), the start position of the filaments moves slightly away from the focusing lens as the turbulent action area increases. We suppose that the move is attributed to the cumulative effect of turbulence increasing as the turbulent action area expands. Based on the observations from Figs. 2(a) and 2(b), it is evident that when the turbulence refractive index structure constant is $2.5 \times 10^{-11}\ \mathrm{m}^{-2/3}$ and the turbulent action area extends to 30 m, the start position of the filament undergoes a displacement of approximately 5 cm towards the direction of laser propagation, in contrast to its start position in the laboratory environment.

Furthermore, the variations of turbulence intensity and turbulence region influence the length of the femtosecond laser filament. Hence, we derive an estimation for the length of the femtosecond laser filaments in turbulence, indicated as the black curve in Fig. 2(c). Figure 2(c) presents the filament lengths measured at various turbulence intensities, demonstrating a notable reduction in the length of the femtosecond laser filament under turbulent conditions. It is evident that the relationship between the filament length and the structure constant of the turbulent refractive index does not exhibit a linear decrease. It is worth noting that the change of the turbulence region does not alter the relationship between filament length and turbulence intensity (Fig. S2 in Supplementary Material). The relationship between the turbulent refractive index structure constant and the length of the filament has been studied theoretically and reported, i.e., the length of the filament can be estimated using the following formula[25]:

$$L_f = L_r \times \left(\frac{1.1 \ln(0.81(P/P_c))}{1 + 0.3(f/L_r)^{-2.5}} \right), \quad (1)$$

where $L_r = k_0 a^2$, $k_0 = 2\pi/\lambda$ is the wavenumber, and a is the radius of the beam profile at the 1/e level of intensity. Figure 2(c) indicates that the experimental and theoretical results are in good agreement.

We subsequently investigate the influence of turbulent action regions on the length of filaments under two experimental conditions: maximum and minimum turbulence refractive index structure constants. Figure 2(d) demonstrates that the increase of the turbulent action region leads to a further reduction in the length of the filament. Based on the findings from Fig. 2(c), when the turbulence refractive index structure constant reaches $2.5 \times 10^{-11}\ \mathrm{m}^{-2/3}$ and the turbulence region expands to 30 m, the length of the filament measures as about 19 cm. The length is reduced by approximately 10 cm compared to the filament in the laboratory environment without artificial turbulence (corresponding to $1.68 \times 10^{-12}\ \mathrm{m}^{-2/3}$). It is worth noting that for turbulence region 30 m and refractive index structure constant $2.5 \times 10^{-11}\ \mathrm{m}^{-2/3}$, the length of the filament in Fig. 2(c) is slightly different from the filament length in Fig. 2(d). The small difference in the values may be because the two data were obtained from two different experimental measurements. Our estimation attributes this reduction primarily to the alteration of the filament formation threshold power in the presence of turbulence.

Air turbulence not only leads to an increase in the distance required for the chirp pulse to form the filament, but also causes an increased random drift in the center of the filament when the turbulence occurs. Chin's group conducted experimental characterization of the drift of various distances from the center of the filament[26]. The experimental results revealed the absence of correlation between the displacements of the filament in the x and y directions. Additionally, it is proposed that the displacement of the filament center follows the Rayleigh distribution law. Here, our focus is directed toward investigating the influence of turbulence intensity and the region affected by turbulence on the center drift of filaments during the remote propagation of femtosecond laser pulses over a distance of 30 m. Moreover, the pointing stability of optical filaments has been quantified by calculating the standard deviation of the beam center position recorded in Fig. 1(c). The beam center coordinates (x_c, y_c) are calculated according to[27]

$$x_c = \sum_x \sum_y x \cdot S(x,y) / \sum_x \sum_y S(x,y), \quad (2a)$$

$$y_c = \sum_x \sum_y y \cdot S(x,y) / \sum_x \sum_y S(x,y), \quad (2b)$$

where S indicates the intensity of the pixel.

Figure 3(a) presents the observed drift of the standard deviation pertaining to the transverse displacement of the femtosecond laser filament as the turbulence refractive index structure constant increases from $1.68 \times 10^{-12}\ \mathrm{m}^{-2/3}$ to $2.5 \times 10^{-11}\ \mathrm{m}^{-2/3}$. Notably, the enhanced turbulence refractive index structure constant amplifies the drift of the filament. Additionally, a linear relationship is observed between the recorded standard deviation and the square root of the turbulence refractive index structure constant, demonstrating a satisfactory linear fit, which forms an empirical formula as follows:

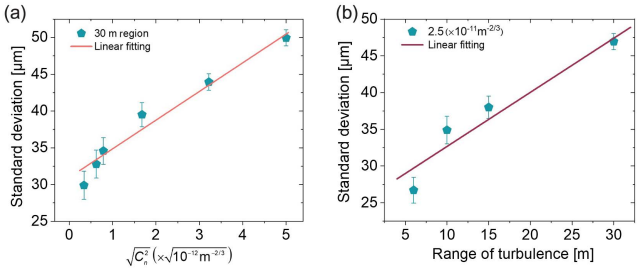

Fig. 3. (a) Dependence of standard deviation of transverse displacement of the filament on the turbulence refractive index structure constant in 30 m region; (b) dependence of standard deviation of transverse displacement of the filament on the turbulence region with $C_n^2 = 2.5 \times 10^{-11}\ \mathrm{m}^{-2/3}$.

$$\langle \delta \rangle = k \times \sqrt{C_n^2}. \quad (3)$$

Importantly, it is worth emphasizing that the alteration of the turbulence region does not affect the relationship between the standard deviation of the transverse displacement of the filament and the turbulence intensity (Fig. S3 in Supplementary Material).

We subsequently explore the impact of turbulent action regions on the standard deviation of the transverse displacement of filaments under maximum turbulence refractive index structure constants. Figure 3(b) reveals that the expansion of the turbulent region leads to an increase in filament drift. Moreover, the standard deviation of filament drift exhibits a linear relationship with the enlargement of the turbulent region. This observation suggests that the cumulative effect on filament drift due to the turbulent region expansion follows a linear trend.

Next, we direct our attention to the influence of turbulence on the cross-sectional effective area of femtosecond laser filamentation. In Fig. 4(a), the diameter of the filament cross section exhibits a gradual increment as the turbulence refractive index structure constant escalates from $1.68 \times 10^{-12}\ \mathrm{m}^{-2/3}$ to $2.5 \times 10^{-11}\ \mathrm{m}^{-2/3}$, considering a turbulent action region of 30 m. It is noteworthy that due to the nonstandard circular shape of the filament cross section, we utilize the average of the sum of diameters in both the transverse and longitudinal directions as the effective diameter of the filament cross section. Furthermore, as the turbulence refractive index structure constant increases, Fig. 4(a) demonstrates the increase of wavefront instability caused by atmospheric turbulence, resulting in the formation of multiple filaments within the femtosecond laser. This observation aligns with previously reported findings, corroborating the consistency of our results[28]. As can be seen in Fig. 4(a), the femtosecond laser filament has formed a multifilament

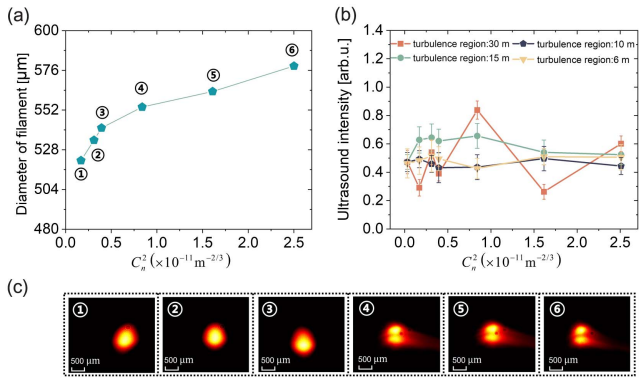

Fig. 4. (a) Dependence of diameter of filament on turbulence refractive index structure constant in 30 m region; (b) dependence of intensity of filament on turbulence refractive index structure constant in different regions; (c) shapes of the filament cross sections corresponding to numbers in (a).

when the turbulence refractive index structure constant is $8.37 \times 10^{-12}\ \mathrm{m}^{-2/3}$.

Lastly, we explor the impact of turbulence intensity on the intensity of the femtosecond laser filament. Employing the setup depicted in Fig. 1(b), the radiated ultrasound signal intensity of the filament was recorded at various turbulence intensities, as depicted in Fig. 4(b). Figure 4(b) demonstrates that alterations within the turbulent region, as well as variations in turbulence intensity, do not affect the intensity of the femtosecond laser filament. This phenomenon can primarily be attributed to the influence of turbulence on the formation threshold of the femtosecond laser filament, resulting in a corresponding alteration in the filament length. In the presence of turbulence, filaments formed exhibit a consistent intensity that remains unaffected by the turbulence. In Fig. 4(b), for the turbulence region 30 m, the ultrasound intensity oscillates strongly with the turbulent refractive index structure constant. This is mainly due to the fact that the wandering of the filament in the cross section increases with the increase of the turbulent refractive index structure constant, as shown in Fig. 3. This leads to a shake in the relative position between the filament and the ultrasound probe, which affects the collection efficiency of the probe and ultimately leads to a stronger oscillation in the intensity of the collected ultrasound signal.

4. Conclusion

In this paper, we have conducted experimental investigations on the impact of turbulence intensity and turbulence action region on various characteristics of femtosecond laser filaments. Specifically, the onset position, length, intensity, and cross-sectional diameter of these filaments were explored. By analyzing the ultrasonic signals emitted by the filaments, it is observed that increasing turbulence intensity and expanding turbulent action area cause the onset of the filament to shift toward the direction of laser propagation, resulting in shorter filament length. Remarkably, these experimental findings align with theoretical calculations. Furthermore, it is observed that as the turbulence refractive index structure constant transitions from $1.68 \times 10^{-12}\ \mathrm{m}^{-2/3}$ to $2.5 \times 10^{-11}\ \mathrm{m}^{-2/3}$, the effective cross-sectional area of the femtosecond laser filament increases. Additionally, when the turbulence refractive index structure constant reaches $8.37 \times 10^{-12}\ \mathrm{m}^{-2/3}$, multiple filaments are formed. Moreover, we have discovered a linear relationship between the standard deviation of the drift displacement of the femtosecond laser filament in its cross section and the square root of the turbulent refractive index structure constant. Interestingly, it was determined that turbulence does not significantly affect the intensity of the femtosecond laser filament. Our findings provide valuable insights into the behavior of femtosecond laser propagation in complex environments, specifically atmospheric turbulence. These results contribute to the comprehension of long-range propagation mechanisms in complex atmospheric conditions. Furthermore, the results offer guidance for remote-sensing and imaging applications aimed at detecting and analyzing multicomponent pollutants and targets.

Acknowledgement

This work was supported by the National Key Research and Development Program of China (No. 2018YFB0504400) and the Fundamental Research Funds for the Central Universities (No. 63223052).

†These authors contributed equally to this work.

References

1. S. L. Chin, S. A. Hosseini, W. Liu, Q. Luo, F. Théberge, N. Akozbek, A. Becker, V. P. Kandidov, O. G. Kosareva, and H. Schroeder, "The propagation of powerful femtosecond laser pulses in optical media: physics, applications, and new challenges," Can. J. Phys. **83**, 863 (2005).
2. A. Couairon and A. Mysyrowicz, "Femtosecond filamentation in transparent media," Phys. Rep. **441**, 47 (2007).
3. J. Kasparian and J. P. Wolf, "Physics and applications of atmospheric nonlinear optics and filamentation," Opt. Express **16**, 466 (2008).
4. P. Qi, L. Lin, Q. Su, N. Zhang, L. Sun, and W. Liu, "*In-situ* visualization of multiple filament competition dynamic during nonlinear propagation of femtosecond laser," Sci. Rep. **7**, 10384 (2017).
5. J. Kasparian, M. Rodriguez, G. Méjean, J. Yu, E. Salmon, H. Wille, R. Bourayou, S. Frey, Y.-B. André, A. Mysyrowicz, R. Sauerbrey, J.-P. Wolf, and L. Wöste, "White-light filaments for atmospheric analysis," Science **301**, 61 (2003).
6. M. Rodriguez, R. Bourayou, G. Méjean, J. Kasparian, J. Yu, E. Salmon, A. Scholz, B. Stecklum, J. Eislöffel, U. Laux, A. P. Hatzes, R. A. Sauerbrey, L. Wöste, and J. P. Wolf, "Kilometer-range nonlinear propagation of femtosecond laser pulses," Phys. Rev. E **69**, 036607 (2004).
7. H. Xu, Y. Cheng, S. L. Chin, and H. Sun, "Femtosecond laser ionization and fragmentation of molecules for environmental sensing," Laser Photon. Rev. **9**, 275 (2015).
8. S. L. Chin, H. L. Xu, Q. Luo, F. Théberge, W. Liu, J.-F. Daigle, Y. Kamali, P. T. Simard, J. Bernhardt, S. A. Hosseini, M. Sharifi, G. Méjean, A. Azarm, C. Marceau, O. G. Kosareva, V. P. Kandidov, N. Aközbek, A. Becker, G. Roy, P. Mathieu, J.-R. Simard, M. Châteauneuf, and J. Dubois, "Filamentation 'remote' sensing of chemical and biological agents/pollutants using only one femtosecond laser source," Appl. Phys. B **95**, 1 (2009).

9. H. L. Xu, G. Méjean, W. Liu, Y. Kamali, J.-F. Daigle, A. Azarm, P. T. Simard, P. Mathieu, G. Roy, J.-R. Simard, and S. L. Chin, "Remote detection of similar biological materials using femtosecond filament-induced breakdown spectroscopy," Appl. Phys. B **87**, 151 (2007).
10. W. Liu, F. Théberge, J.-F. Daigle, P. T. Simard, S. M. Sarifi, Y. Kamali, H. L. Xu, and S. L. Chin, "An efficient control of ultrashort laser filament location in air for the purpose of remote sensing," Appl. Phys. B **85**, 55 (2006).
11. H. Gao, W. Chu, G. Yu, B. Zeng, J. Zhao, Z. Wang, W. Liu, Y. Cheng, and Z. Z. Xu, "Femtosecond laser filament array generated with step phase plate in air," Opt. Express **21**, 4612 (2013).
12. C. Chu, D. E. Shipilo, D. Lu, Z. Zhang, S. V. Chuchupal, N. A. Panov, O. G. Kosareva, and W. Liu, "Femtosecond filament emergence between π-shifted beamlets in air," Opt. Express **28**, 1002 (2020).
13. J. Guo, L. Sun, J. Liu, B. Shang, S. Tao, N. Zhang, L. Lin, and Z. Zhang, "Beam wander restrained by nonlinearity of femtosecond laser filament in air," Sensors **22**, 4995 (2022).
14. B. Yan, D. Li, L. Zhang, T. Xi, Y. Cai, and Z. Hao, "Filamentation of femtosecond vortex laser pulses in turbulent air," Opt. Laser Technol. **164**, 109515 (2023).
15. G. Paunescu, G. Spindler, W. Riede, H. Schröder, and A. Giesen, "Multifilamentation of femtosecond laser pulses induced by small-scale air turbulence," Appl. Phys. B **96**, 175 (2009).
16. E. Silaeva, S. Shlenov, and V. P. Kandidov, "Multifilamentation of high-power femtosecond laser pulse in turbulent atmosphere with aerosol," Appl. Phys. B **101**, 393 (2010).
17. Y.-Y. Ma, X. Lu, T. Xi, Q. Gong, and J. Zhang, "Widening of Long-range femtosecond laser filaments in turbulent air," Opt. Express **16**, 8332 (2008).
18. V. P. Kandidov, O. G. Kosareva, M. P. Tamarov, A. Brodeur, and S. L. Chin, "Nucleation and random movement of filaments in the propagation of high-power laser radiation in a turbulent atmosphere," Quantum. Electron. **29**, 911 (1999).
19. J. R. Peñano, B. Hafizi, A. C. Ting, and M. H. Helle, "Theoretical and numerical investigation of filament onset distance in atmospheric turbulence," J. Opt. Soc. Am. B **31**, 963 (2014).
20. Y. Hu, J.-S. Nie, K. Sun, and L. Wang, "Filamentation of femtosecond laser pulse influenced by the air turbulence at various propagation distances," Opt. Commun. **383**, 281 (2017).
21. A. Houard, M. Franco, B. S. Prade, A. Durécu, L. Lombard, P. Bourdon, O. J. Vasseur, B. Fleury, C. Robert, V. Michau, A. Couairon, and A. Mysyrowicz, "Femtosecond filamentation in turbulent air," Phys. Rev. A **78**, 033804 (2008).
22. S. A. Hosseini, J. Yu, Q. Luo, and S. L. Chin, "Multi-parameter characterization of the longitudinal plasma profile of a filament: a comparative study," Appl. Phys. B **79**, 519 (2004).
23. S. Bendersky, N. S. Kopeika, and N. Blaunstein, "Atmospheric optical turbulence over land in middle east coastal environments: prediction modeling and measurements," Appl. Opt. **43**, 4070 (2004).
24. P. Qi, W. Qian, L. Guo, J. Xue, N. Zhang, Y. Wang, Z. Zhang, Z. Zhang, L. Lin, C. Sun, L. Zhu, and W. Liu, "Sensing with femtosecond laser filamentation," Sensors **22**, 7076 (2022).
25. A. A. Zemljanov, A. D. Bulygin, and O. V. Minina, "Filamentation length for femtosecond laser radiation focused by conic and parabolic lenses," Russ. Phys. J. **56**, 286 (2013).
26. S. L. Chin, A. Talebpour, J. Yang, S. Petit, V. P. Kandidov, O. G. Kosareva, and M. P. Tamarov, "Filamentation of femtosecond laser pulses in turbulent air," Appl. Phys. B **74**, 67 (2002).
27. J. Yang, T. Zeng, L. Lin, and W. Liu, "Beam wandering of femtosecond laser filament in air," Opt. Express **23**, 25628 (2015).
28. T. Zeng, H. Gao, X. D. Sun, L. Lin, and W. Liu, "Generation of multiple femtosecond laser filaments by using axicon in turbulent air," Laser Phys. **25**, 085401 (2015).